



## Sensing behavior of flower-shaped MoS<sub>2</sub> nanoflakes: case study with methanol and xylene

Maryam Barzegar<sup>1</sup>, Masoud Berahman<sup>2</sup> and Azam Irajizad<sup>\*1,2</sup>

### Full Research Paper

Open Access

Address:

<sup>1</sup>Nanotechnology Research Institute, Sharif University of Technology, Tehran, Iran and <sup>2</sup>Physics Department, Sharif University of Technology, Tehran, Iran

Email:

Azam Irajizad<sup>\*</sup> - Irajizad@sharif.ir

\* Corresponding author

Keywords:

density functional theory; gas sensor; hydrothermal method; methanol; MoS<sub>2</sub> nanoflakes; xylene vapor

*Beilstein J. Nanotechnol.* **2018**, *9*, 608–615.

doi:10.3762/bjnano.9.57

Received: 01 August 2017

Accepted: 26 January 2018

Published: 16 February 2018

Associate Editor: N. Motta

© 2018 Barzegar et al.; licensee Beilstein-Institut.

License and terms: see end of document.

### Abstract

Recent research interest in two-dimensional (2D) materials has led to an emerging new group of materials known as transition metal dichalcogenides (TMDs), which have significant electrical, optical, and transport properties. MoS<sub>2</sub> is one of the well-known 2D materials in this group, which is a semiconductor with controllable band gap based on its structure. The hydrothermal process is known as one of the scalable methods to synthesize MoS<sub>2</sub> nanostructures. In this study, the gas sensing properties of flower-shaped MoS<sub>2</sub> nanoflakes, which were prepared from molybdenum trioxide (MoO<sub>3</sub>) by a facile hydrothermal method, have been studied. Material characterization was performed using X-ray diffraction, Brunauer–Emmett–Teller surface area measurements, elemental analysis using energy dispersive X-ray spectroscopy, and field-emission scanning electron microscopy. The gas sensing characteristics were evaluated under exposure to various concentrations of xylene and methanol vapors. The results reveal higher sensitivity and shorter response times for methanol at temperatures below 200 °C toward 200 to 400 ppm gas concentrations. The sensing mechanisms for both gases are discussed based on simulation results using density functional theory and charge transfer.

### Introduction

Recent efforts in exploring two-dimensional (2D) materials have led to the introduction of a new family of materials known as transition metal dichalcogenides (TMDs), which show remarkable electrical, optical and transport properties [1-13]. TMDs are a group of materials with the general formula MX<sub>2</sub>, where M is a transition metal element of group IV, V or VI, and X is a chalcogen (S, Se, or Te) [1-13]. Their properties, includ-

ing a large surface-to-volume ratio, high process compatibility and flexibility, make them good candidates for sensing applications [8,14,15]. One of the most explored materials in this group is MoS<sub>2</sub>, which is a semiconductor with a variable band gap based on the number of layers [14,15]. Numerous methods have been applied to synthesize single or few-layered MoS<sub>2</sub>, including but not limited to mechanical cleavage, chemical exfolia-

tion, hydrothermal synthesis and chemical vapor deposition [16–23]. The hydrothermal process is a scalable method to synthesize MoS<sub>2</sub> nanosheets and nanoflakes. There are numbers of articles which report the successful growth of flower-like MoS<sub>2</sub> nanoflakes using this technique [19–23]. Due to the high surface-to-volume ratio, activity, tunable band gap, low electrical noise and acceptable electrical conductivity, MoS<sub>2</sub> is considered as one of the most suitable candidates to use in gas sensing devices [14,15].

There are few reports on gas sensing properties of MoS<sub>2</sub>. Cantalini et al. [8] reported the response of few layer MoS<sub>2</sub> films to NO<sub>2</sub> at sub-ppm concentrations and reasonable sensitivity to 1 ppm NO<sub>2</sub> with fast and reversible response at 100 °C. It has been shown that charge transfer between MoS<sub>2</sub> and NO<sub>2</sub> or NH<sub>3</sub> molecules can be considered as the main reason behind the changes in resistance [24]. In another report, the remarkable potential of MoS<sub>2</sub> in sensing triethylamine molecules has been investigated. It has been shown that MoS<sub>2</sub> is a good sensor to detect acetone with response to methanol [14]. There are also investigations that marked the high response of MoS<sub>2</sub> toward methanol and ethanol [15]. Besides these experimental reports, there are numerous theoretical investigations which illustrate the potential of MoS<sub>2</sub> for detecting various gas molecules [25,26]. Among these reports, the properties of flower-shaped MoS<sub>2</sub> as a gas sensor is underestimated, hence in this paper, we demonstrate this potential. The flower-shaped MoS<sub>2</sub> can easily be grown using the inexpensive hydrothermal technique with high quality and in large quantity, which reduces the final cost of the sensor. To demonstrate this potential, we consider xylene and methanol molecules as the target gases.

Xylene is a nonpolar colorless flammable gas that not only pollutes the environment but is also directly harmful to human health as a carcinogenic gas. Since xylene exists in the mixture of gasoline, in the solvent components of commonly used commercial products, and in some paint and varnishes, monitoring the existence of this gas in the related industries is of vital importance [27–30]. Methanol, on the other hand, is a polar, colorless, flammable molecule which is highly toxic for human both in liquid and vapor form. The inhalation of methanol vapor may cause serious problems for metabolism, which highlights the importance of monitoring this gas in the environment [27–30].

In this paper, we explore the gas sensing potential of pure flower-shaped MoS<sub>2</sub> nanoflakes toward xylene and methanol vapors. We show that these flower-shaped MoS<sub>2</sub> nanoflakes have adequate surface-to-volume ratio and active surface sites to detect gas molecules and our results reveal that they can detect methanol and xylene with good response.

This paper is organized as follows: in the Experimental and Simulation section, details of the growth and the setup of our research are discussed. In addition, the resulting MoS<sub>2</sub> nanoflakes are characterized. The simulation process is also discussed in this section. In the Results and Discussion section, our results on gas sensing properties of the produced MoS<sub>2</sub> toward xylene and methanol are presented. In addition, the selectivity of our device toward various available gas molecules and the mechanism of adsorption as well as the simulation results are discussed.

## Experimental and Simulation Data

### Synthesis of MoS<sub>2</sub> few-layer nanoflakes

Among various methods for preparing MoS<sub>2</sub> few-layer sheets, we followed the synthesis process reported before in [23]. In short, the MoS<sub>2</sub> sheets were synthesized through sulfurization of MoO<sub>3</sub> powder in an aqueous medium as follows: 0.05 g MoO<sub>3</sub> powder and 0.13 g thiourea were dissolved in 40 mL deionized water followed by rapid stirring for about 30 min. Subsequently, the mixture was transferred into a 50 mL teflon-lined stainless steel autoclave and maintained at 200 °C for 24 h. After cooling naturally, the black MoS<sub>2</sub> product was collected by filtration, washed with distilled water and pure ethanol for several times and then dried under vacuum at 45 °C overnight.

### Characterization

X-ray diffraction (XRD) patterns were obtained with an X-ray diffractometer (Shimadzu XRD-6000, Cu K $\alpha$  radiation) and energy dispersive X-ray (EDX) spectra and sample morphology were characterized by field-emission scanning electron microscopy (FE-SEM, TE-SCAN, MIRA3). The Brunauer–Emmett–Teller (BET) surface area of the products was analyzed using a Micromeritics nitrogen adsorption apparatus.

### Fabrication of gas sensors

An alumina wafer with an area of 1 cm<sup>2</sup> was considered as the proper substrate for our gas sensors. The substrates were immersed in acetone and isopropyl alcohol and sonicated for 15 min to remove any undesired surface ions. A 200 nm Pt film as a snake-shaped heater was sputtered on the back of the substrate using a sputter coater from Nanostructured Coatings Co. To fabricate the sensor device, dispersed flower-shaped MoS<sub>2</sub> nanoflakes in ethanol were first deposited on a 1 × 1 cm<sup>2</sup> alumina wafer by spin coating. Then the gold microelectrodes were deposited on selective areas of the prepared, uniform, thin film through a comb-shaped shadow mask by sputtering. The mask was then lifted off and the microelectrodes with 100  $\mu$ m width and a 200  $\mu$ m gap between each electrode remained and were annealed at 200 °C for 120 min for better film adhesion.

## Gas sensing measurements

In order to test the samples toward different gas molecules, a dynamic system based on  $N_2$  as a carrier gas is used. For testing the sensor operation, the target vapors were produced by bubbling dry air through the respective solvents. The amount of xylene and methanol as target gases were controlled by two mass flow controllers. The concentration of xylene and methanol was calculated using Equation 1 [30]:

$$c \text{ (ppm)} = 10^6 \times \left( \frac{P_s}{P} \times \frac{f}{f+F} \right), \quad (1)$$

where  $f$  and  $F$  are the flow rates (in sccm) of the bubbling  $N_2$  saturated with the vapors and the  $N_2$  gas, respectively;  $P$  is the total pressure and  $P_s$  is the saturated vapor partial pressure obtained by the Antoine equation [31]. Special care with regards to temperature control was taken so that the formula is valid in our system throughout the testing period.

The chemoresistance response is defined as  $(R_{\text{air}} - R_{\text{gas}})/R_{\text{air}}$  where  $R_{\text{air}}$  and  $R_{\text{gas}}$  are the resistance in  $N_2$  and the mixed gases in different concentrations, respectively.

## Simulation

A super-cell containing 25 primitive unit cells of monolayer  $MoS_2$  was considered as the pristine model. Then, a sulfur atom at the center of the model was removed and fully relaxed to study the sulfur vacancy. After that, the detection of xylene and methanol with these models were studied. Density functional theory in the local-density approximation with a Perdew–Zunger correlation function was considered in a double-zeta polarized scheme with a mesh cut-off sampling of 75 Ry for optimization and study [32]. The Monkhorst–Pack mesh with  $21 \times 21 \times 1$  sampling was used for the investigation. The optimization process continued until the force on each atom was lower than 0.01 eV. The Grimme–DFT–D2 method was used to model the van der Waals interactions that may occur in the simulation. All calculations are performed using the well-known siesta package [33,34].

## Results and Discussion

The crystalline structure and phase purity of the dried black  $MoS_2$  powder were investigated using XRD. As illustrated in Figure 1, there are two completely distinguishable peaks at  $33.61^\circ$  and  $59.19^\circ$  which are in good agreement with corresponding peaks of the (100) and (110) planes of  $MoS_2$  sheets with hexagonal crystal structure denoted as the 2H phase (JCPDS-37-1492). The measured  $d$ -spacings of 0.26 nm and 0.15 nm are related to the (100) and (110) planes, respectively.

The broadening of the XRD peaks may indicate nanometer-size growth of  $MoS_2$  with few-layer stacks.

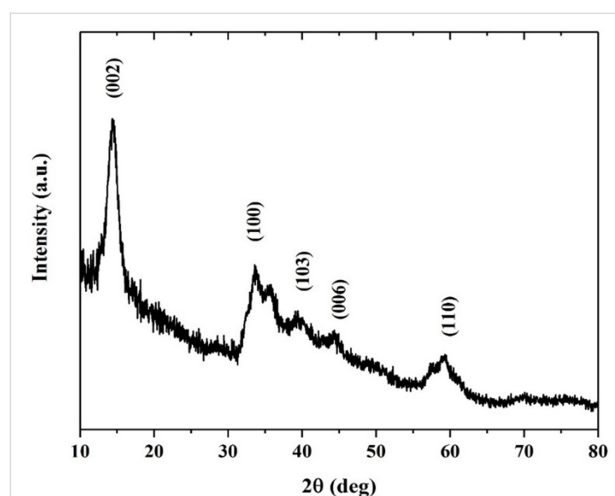


**Figure 1:** The X-ray diffraction pattern of flower-shaped  $MoS_2$  nanoflakes synthesized by the hydrothermal method.

In order to confirm such results, the size and morphology of the prepared  $MoS_2$  samples were observed using FE-SEM as shown in Figure 2a, and in higher magnification in Figure 2b. As shown in the micrographs, flower-like particles are grown from few stacking nanoflakes with almost 20 nm thickness. To further investigate the quality of these growth structures, EDX data were obtained.

Figure 3 shows an S to Mo atomic ratio of about 1.87, indicating sulfur vacancies in the samples. The previous report shows that sulfur vacancies can increase the possibility of charge transfer in  $MoS_2$  nanoflakes which may act as the main reason to alter the conductivity [35]. It has been also reported that the crystal phase and edge play a significant role in the electro-activity of  $MoS_2$  nanosheets. Furthermore, sulfur vacancies contribute significantly to the electronic properties of  $MoS_2$  [36,37]. Hence, such sulfur vacancy is desirable for the gas sensing properties of  $MoS_2$ .

To study the application of the flower-shaped  $MoS_2$  for gas sensing, the Brunauer–Emmett–Teller (BET) experiment has been performed. The measured surface area is  $64.14 \text{ m}^2 \text{ g}^{-1}$ , which is more than two times higher compared with the bulk  $MoS_2$  (average  $27 \text{ m}^2 \text{ g}^{-1}$ ) [38].

Figure 4 shows the dynamic response of the fabricated sensor to different concentrations of methanol vapor at working temperatures in the range of 100 to 200 °C. A very small response towards target gases was observed at a temperature below 100 °C. As the sensor is exposed to concentrations of methanol

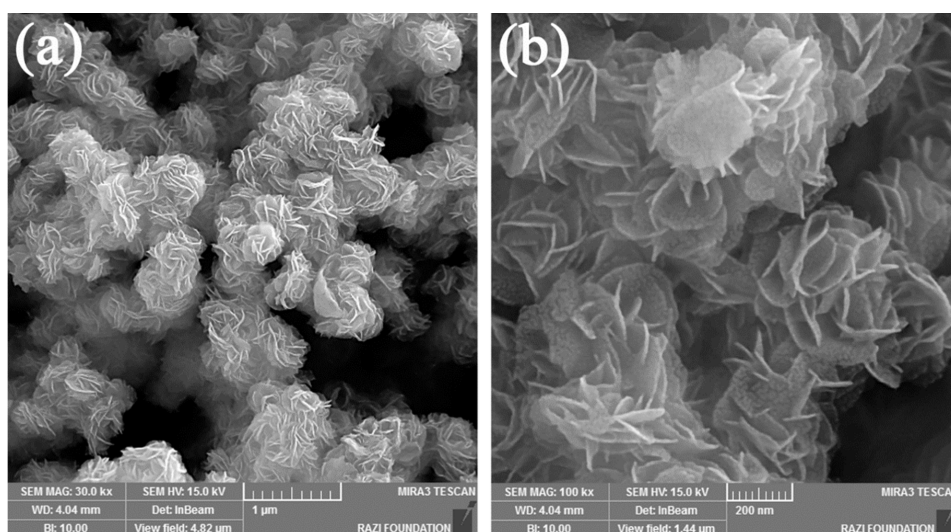


**Figure 2:** FE-SEM micrographs of flower-shaped MoS<sub>2</sub> nanoflakes synthesized via the hydrothermal method.

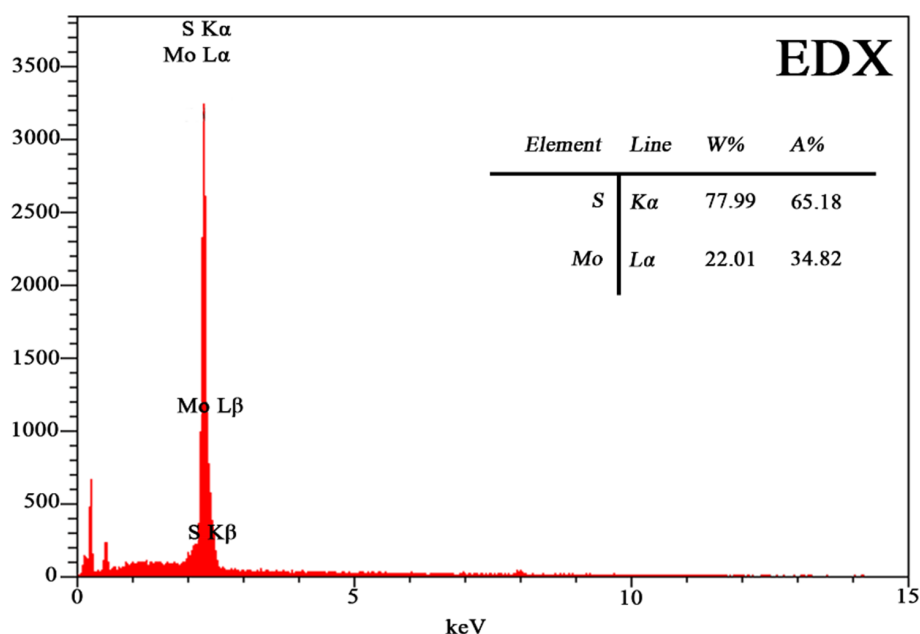


**Figure 3:** EDX analysis of MoS<sub>2</sub> nanoflake powder as prepared by the aqueous hydrothermal method.

in the range of the health exposure limits (i.e., 200–400 ppm), it reacts quickly and the resistance reduces. Figure 4a clearly illustrates the reversible behavior of about 120 s and 370 s as the response and recovery times for 200 ppm, respectively. When the working temperature was increased, the sensitivity was improved from 25 to 55 for 200 °C and the response time decreased from about 800 s to 120 s (Figure 4b).

In addition, we studied the sensing ability of the flower-shaped MoS<sub>2</sub> nanosheets toward xylene. Figure 5a,b represents the gas

sensing response toward 200–400 ppm of xylene vapor at the temperature range from 100 to 200 °C. When the temperature was increased, the sensitivity was enhanced from about 0.25 to almost 3 for 400 ppm xylene, while the response and recovery time decreased from about 250 and 500 s to 150 and 450 s, respectively. As illustrated in Figure 5a, when increasing the concentration at 200 °C from 200 to 400 ppm, the sensitivity was improved from 1 to 3, which represents the potential of the fabricated sensor in detecting different concentrations of xylene.

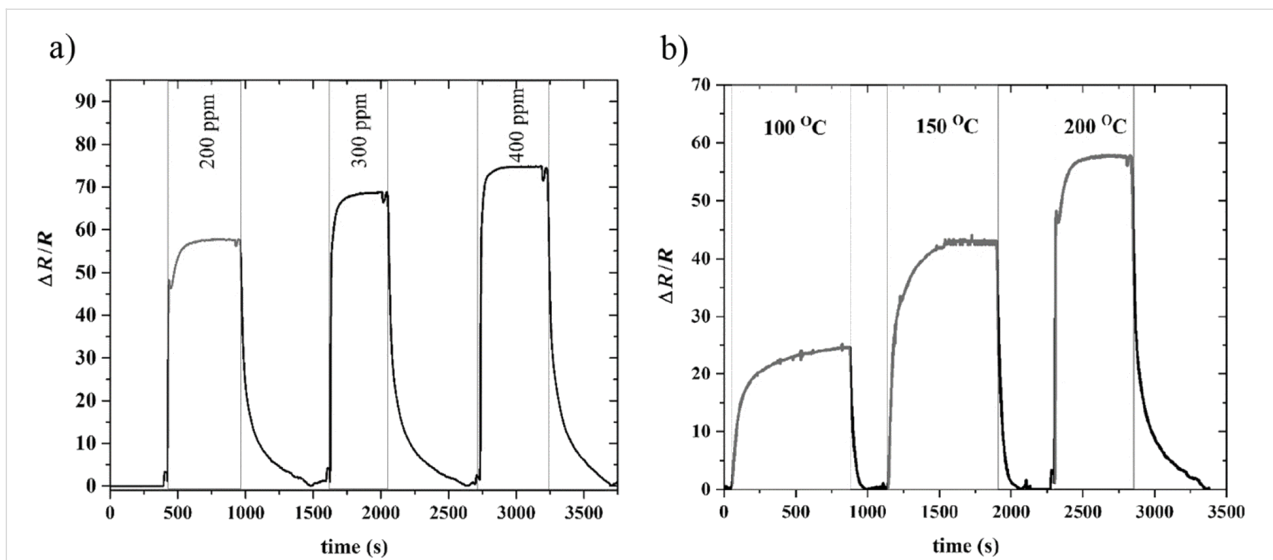


**Figure 4:** Typical response of MoS<sub>2</sub> nanoflakes toward methanol for: (a) different concentrations at 200 °C working temperature, (b) for 200 ppm at different working temperatures.

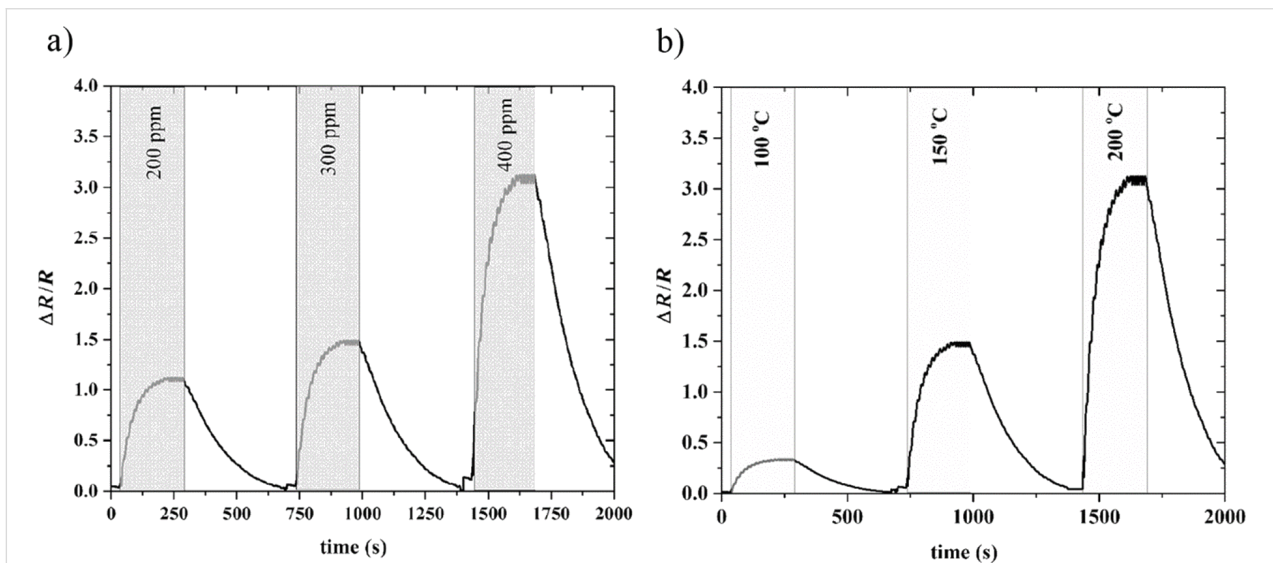
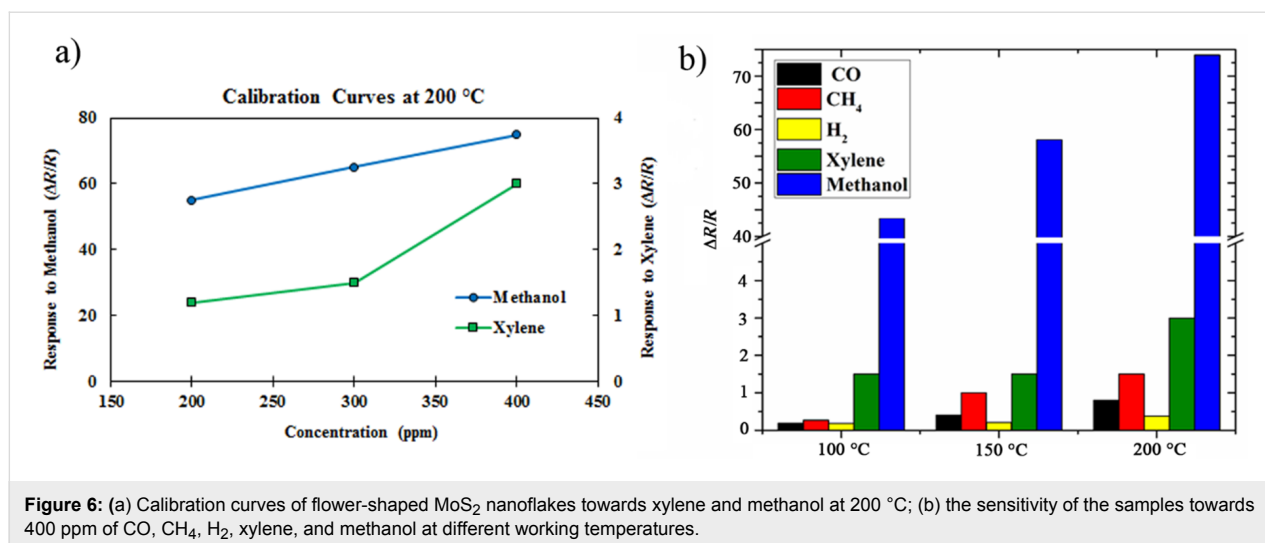


**Figure 5:** Typical response of MoS<sub>2</sub> nanoflakes toward xylene for: (a) different concentrations at 200 °C working temperature, (b) for 400 ppm at different working temperatures.

As indicated in Figure 6a, it is clear that the sensor responds to both methanol and xylene gases, while the former is more linear with higher sensitivity. In order to study the selectivity of our sensor toward available gases in the laboratory, the response toward 400 ppm concentration of H<sub>2</sub>, CH<sub>4</sub> and CO has also been studied. Figure 6b indicates that the sensor is less sensitive than methanol at all working temperatures. It is worth mentioning that when increasing the temperature up to 200 °C, the sensitivity of our samples increased. This response enhancement can be interpreted as methanol decomposition to syngas (CO/H<sub>2</sub>) at around 433 K [39], and ethanol formation from the

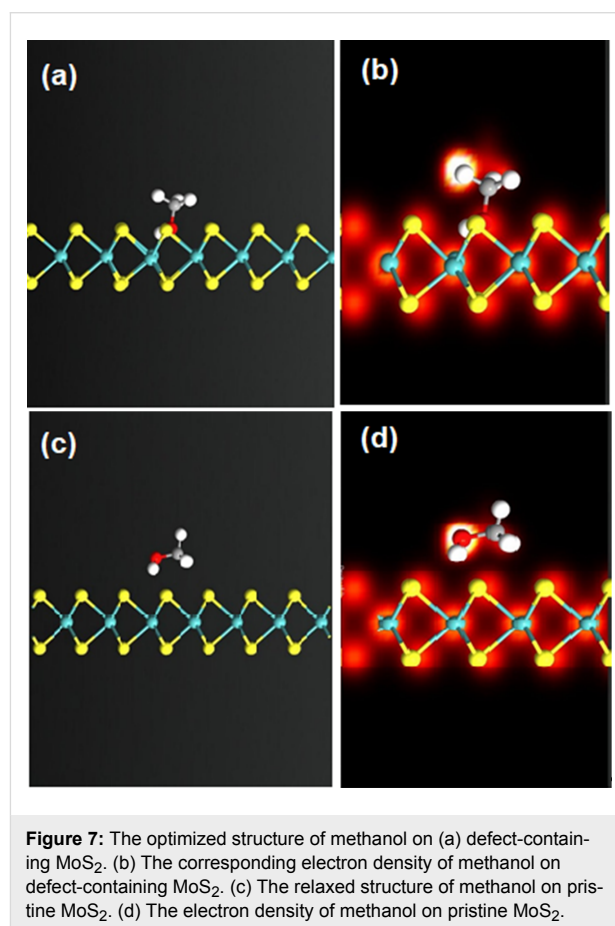
syngas due to the catalytic properties of MoS<sub>2</sub> at around 185 °C [40]. It is known that ethanol has a higher electron-donor rate than methanol [41]. Hence, a larger variation in sample resistance at higher temperatures can be expected.

To study the reason behind this repeatable behavior toward both gases, we consider the flower-shaped MoS<sub>2</sub> as an n-type semiconductor due to its bulk shape, which was also confirmed using Hall effect experiments. Four Ti (10 nm)/Au (200 nm) films as electrodes in van der Pauw configuration were deposited on spin-coated MoS<sub>2</sub>/SiO<sub>2</sub> (300 nm)/Si samples for



Hall effect measurements. The details of the configuration are given in [42]. The results show an n-type characteristic for the samples with an electron density and a mobility of about  $6.3 \times 10^{13} \text{ cm}^{-3}$  and  $75 \text{ cm}^2 \text{ V}^{-1} \text{ s}^{-1}$ , respectively. When xylene vapor (as an electron donor) is exposed to the sensing device, it reduces the resistance of the device due an increase in the majority carrier concentration. The same process can be seen for methanol, acting as powerful electron-donor gas molecules. This increment in the electron carrier concentration can reduce the resistivity of the device. When the gas leaves the chamber, the molecules which transfer the charge from weak van der Waals interaction leave the MoS<sub>2</sub> layer and the concentration of the carrier reduces, hence the resistance returns back to its initial value. In the hydrothermal growth of MoS<sub>2</sub> (as proven before), the high edges, corners and vacancies provide proper sites for reaction and sensing of the gas molecules [43].

A scrutinized investigation of the results revealed that when methanol enters the chamber, the sensor shows a fast response which is followed by a slow one, while the sensor shows only a slow process toward xylene. It may be related to the existence of one reaction mechanism for xylene as a nonpolar molecule and two distinct mechanisms for methanol as a polar one. To find such differences, we performed a simulation study on the pristine monolayer and similar surface with sulfur vacancy of MoS<sub>2</sub> in the presence of xylene and methanol molecules. Xylene shows almost no interaction with pristine MoS<sub>2</sub> while a van der Waals interaction happens in the case of sulfur vacancy, which leads to charge transfer from xylene to MoS<sub>2</sub>. Since only defect sites can acquire charges from xylene, we expect only one mechanism for gas detection of this kind. Figure 7 illustrates the interaction of methanol on pristine and sulfur-vacancy MoS<sub>2</sub> and the electron density of these materials. As can be seen, methanol can transfer charge via van der Waals interactions



both toward the pristine and the defect-containing MoS<sub>2</sub>. These two different detection sites for methanol can result in two distinct mechanisms that are observed in our experiments. The fast process is related to charge transfer on the pristine sites while the slow one may be related to the physical adsorption of the methanol molecules on the deficient sites. It can be assumed

that the sulfur vacancies can provide active sites for gas molecules to interact with MoS<sub>2</sub> as well as altering the position of sub-bands in the band structure [44].

The Mulliken population shows that the charge transfer in the case of xylene on pristine and the defect-containing MoS<sub>2</sub> is almost 0.001e and 0.027e (average of different isomers), respectively, in the area of study. In the case of methanol, the Mulliken population is 0.04e and 0.071e in the pristine and the defect sites, respectively. These results demonstrate that both xylene and methanol transfer a fraction of a charge to MoS<sub>2</sub>, which lead to an increase in carrier concentration and reduction of sample resistance.

## Conclusion

In summary, we demonstrated a facile and efficient hydrothermal synthesis of MoS<sub>2</sub> nanoflakes. It was found that the nanoflakes form a flower-shaped structure with a large surface-to-volume ratio. The sensor device was successfully fabricated by spin coating of MoS<sub>2</sub> flakes on an alumina substrate, on the back side of which a Pt heater circuit for thermal annealing was deposited. Our results indicate that the produced, flower-shaped MoS<sub>2</sub> nanoflakes showed sensitivity towards methanol and xylene as polar and nonpolar gas molecules. We discussed changes in resistivity toward gas molecules according to a charge transfer mechanism. It was found that both gases can be detected in concentrations as low as 200 ppm while the detection sensitivity increased with increasing gas concentration. It was also confirmed that the response and recovery time for sensors decreased dramatically with increasing temperature. The sensitivity of the produced sensor device towards methanol was found to be higher than for xylene, as the calibration curve indicated a linear response to increasing concentration. In addition, the simulation results showed that xylene interacts with defect sites while methanol can interact with both the pristine and the defect sites, leading to higher sensitivity, which coincides well with the experimental results of this study.

## Acknowledgements

The authors are grateful to the National Elite Foundation of Iran and Iranian National Science Foundation (INSF) for their financial support of the thesis and the research project.

## References

- Wang, Q. H.; Kalantar-Zadeh, K.; Kis, A.; Coleman, J. N.; Strano, M. S. *Nat. Nanotechnol.* **2012**, *7*, 699–712. doi:10.1038/nnano.2012.193
- Chen, D.; Chen, W.; Ma, L.; Ji, G.; Chang, K.; Lee, J. Y. *Mater. Today* **2014**, *17*, 184–193. doi:10.1016/j.mattod.2014.04.001
- Kim, S.; Konar, A.; Hwang, W.; Lee, J. H.; Lee, J.; Yang, J.; Jung, C.; Kim, H.; Yoo, J.-B.; Choi, J.-Y.; Jin, Y. W.; Lee, S. Y.; Jena, D.; Choi, W.; Kim, K. *Nat. Commun.* **2012**, *3*, 1011. doi:10.1038/ncomms2018
- Zhao, Y.; Zhang, Y.; Yang, Z.; Yan, Y.; Sun, K. *Sci. Technol. Adv. Mater.* **2013**, *14*, 043501. doi:10.1088/1468-6996/14/4/043501
- Chhowalla, M.; Shin, H. S.; Eda, G.; Li, L.-J.; Loh, K. P.; Zhang, H. *Nat. Chem.* **2013**, *5*, 263–275. doi:10.1038/nchem.1589
- Sreeprasad, T. S.; Nguyen, P.; Kim, N.; Berry, V. *Nano Lett.* **2013**, *13*, 4434–4441. doi:10.1021/nl402278y
- Enyashin, A. N.; Seifert, G. *Nanosyst.: Phys., Chem., Math.* **2014**, *5*, 517–539.
- Cantalini, C.; Giancaterini, L.; Donarelli, M.; Santucci, S.; Ottaviano, L. NO<sub>2</sub> response to few-layers MoS<sub>2</sub>. International Meeting on Chemical Sensors, Nuremberg: Germany, May 20–23, 2012; 2012; pp 1656–1659. doi:10.5162/IMCS2012/P2.8.4
- Butler, S. Z.; Hollen, S. M.; Cao, L.; Cui, Y.; Gupta, J. A.; Gutiérrez, H. R.; Heinz, T. F.; Hong, S. S.; Huang, J.; Ismach, A. F.; Johnston-Halperin, E.; Kuno, M.; Plashnitsa, V. V.; Robinson, R. D.; Ruoff, R. S.; Salahuddin, S.; Shan, J.; Shi, L.; Spencer, M. G.; Terrones, M.; Windl, W.; Goldberger, J. E. *ACS Nano* **2013**, *7*, 2898–2926. doi:10.1021/nn400280c
- Roy, T.; Tosun, M.; Kang, J. S.; Sachid, A. B.; Desai, S. B.; Hettick, M.; Hu, C. C.; Javey, A. *ACS Nano* **2014**, *6*, 6259–6264. doi:10.1021/nn501723y
- Dolui, K.; Rungger, I.; Sanvito, S. *Phys. Rev. B* **2013**, *87*, 165402. doi:10.1103/PhysRevB.87.165402
- Erementchouk, M.; Khan, M. A.; Leuenberger, M. N. *Phys. Rev. B* **2015**, *92*, 121401. doi:10.1103/PhysRevB.92.121401
- Castellanos-Gomez, A.; van Leeuwen, R.; Buscema, M.; van der Zant, H. S. J.; Steele, G. A.; Venstra, W. J. *Adv. Mater.* **2013**, *25*, 6719–6723. doi:10.1002/adma.201303569
- Perkin, F. K.; Friedman, A. L.; Cobas, E.; Campbell, P. M.; Jernigan, G. G.; Jonker, B. T. *Nano Lett.* **2013**, *13*, 668–673. doi:10.1021/nl3043079
- Samnakay, R.; Jiang, C.; Romyantsev, S. L.; Shur, M. S.; Balandin, A. A. *Appl. Phys. Lett.* **2015**, *106*, 023115. doi:10.1063/1.4905694
- Coleman, J. N.; Lotya, M.; O'Neill, A.; Bergin, S. D.; King, P. J.; Khan, U.; Young, K.; Gaucher, A.; De, S.; Smith, R. J.; Shvets, I. V.; Arora, S. K.; Stanton, G.; Kim, H.-Y.; Lee, K.; Kim, G. T.; Duesberg, G. S.; Hallam, T.; Boland, J. J.; Wang, J. J.; Donegan, J. F.; Grunlan, J. C.; Moriarty, G.; Shmeliov, A.; Nicholls, R. J.; Perkins, J. M.; Grievson, E. M.; Theuwissen, K.; McComb, D. W.; Nellist, P. D.; Nicolosi, V. *Science* **2011**, *331*, 568–571. doi:10.1126/science.1194975
- Li, H.; Wu, J.; Yin, Z.; Zhang, H. *Acc. Chem. Res.* **2014**, *47*, 1067–1075. doi:10.1021/ar4002312
- Song, I.; Park, C.; Choi, H. C. *RSC Adv.* **2015**, *5*, 7495–7514. doi:10.1039/C4RA11852A
- Ren, X.; Pang, L.; Zhang, Y.; Ren, X.; Fan, H.; Liu, S. *J. Mater. Chem. A* **2015**, *3*, 10693–10697. doi:10.1039/C5TA02198G
- Ghatak, S.; Pal, A. N.; Ghosh, A. *ACS Nano* **2011**, *5*, 7707–7712. doi:10.1021/nn202852j
- Schmidt, H.; Wang, S.; Chu, L.; Toh, M.; Kumar, R.; Zhao, W.; Castro Neto, A. H.; Martin, J.; Adam, S.; Özyilmaz, B.; Eda, G. *Nano Lett.* **2014**, *14*, 1909–1913. doi:10.1021/nl4046922
- Wang, S.; Wang, X.; Warner, J. H. *ACS Nano* **2015**, *9*, 5246–5254. doi:10.1021/acsnano.5b00655
- Veeramalai, C. P.; Li, F.; Xu, H.; Kim, T. W.; Guo, T. *RSC Adv.* **2015**, *5*, 57666–57670. doi:10.1039/C5RA07478A

24. Cho, B.; Hahm, M. G.; Choi, M.; Yoon, J.; Kim, A. R.; Lee, Y.-J.; Park, S.-G.; Kwon, J.-D.; Kim, C. S.; Song, M.; Jeong, Y.; Nam, K.-S.; Lee, S.; Yoo, T. J.; Kang, C. G.; Lee, B. H.; Ko, H. C.; Ajayan, P. M.; Kim, D.-H. *Sci. Rep.* **2015**, *5*, 8052. doi:10.1038/srep08052
25. Yue, Q.; Shao, Z.; Chang, S.; Li, J. *Nanoscale Res. Lett.* **2013**, *8*, 425. doi:10.1186/1556-276X-8-425
26. Zhao, S.; Xuea, J.; Kang, W. *Chem. Phys. Lett.* **2014**, *595–596*, 35–42. doi:10.1016/j.cplett.2014.01.043
27. Schaller, E.; Bosset, J. O.; Esher, F. *Lebensm.-Wiss. Technol. (1968-2004)* **1998**, *31*, 305–316. doi:10.1006/fstl.1998.0376
28. Lundström, K. I.; Shivaraman, M. S.; Svenson, C. M. *J. Appl. Phys.* **1975**, *46*, 3876–3881. doi:10.1063/1.322185
29. Wilson, A. D.; Baietto, M. *Sensors* **2009**, *9*, 5099–5148. doi:10.3390/s90705099
30. Buck, T. M.; Allen, F. G.; Dalton, M. *Detection of chemical species by surface effects on metals and semiconductors*; Bell Telephone Laboratories, 1965.
31. Perry, R. H.; Green, D. W.; Maloney, J. O. *Perry's Chemical Engineers Handbook*, 6th ed.; McGraw-Hill: New York, 1984.
32. Perdew, J. P.; Zunger, A. *Phys. Rev. B* **1981**, *23*, 5048. doi:10.1103/PhysRevB.23.5048
33. Soler, J. M.; Artacho, E.; Gale, J. D.; Garcia, A.; Junquera, J.; Ordejón, P.; Sánchez-Portal, D. *J. Phys.: Condens. Matter* **2002**, *14*, 2745–2779. doi:10.1088/0953-8984/14/11/302
34. Li, H.; Huang, M.; Cao, G. *Phys. Chem. Chem. Phys.* **2016**, *18*, 15110–15117. doi:10.1039/C6CP01362G
35. Heinemann, H.; Somorjai, G. A. *Catalysis and Surface Science*; Marcel Dekker Inc.: New York, 1985; p 81.
36. Yin, Y.; Han, J.; Zhang, Y.; Zhang, X.; Xu, P.; Yuan, Q.; Samad, L.; Wang, X.; Wang, Y.; Zhang, Z.; Zhang, P.; Cao, X.; Song, B.; Jin, S. *J. Am. Chem. Soc.* **2016**, *138*, 7965–7972. doi:10.1021/jacs.6b03714
37. Li, J.; Tsai, C.; Koh, A.; Cai, L.; Contryman, A. W.; Fragapane, A. H.; Zhao, J.; Han, H. S.; Manoharan, H. C.; Abild-Pedersen, F.; Nørskov, J. K.; Zheng, X. *Nat. Mater.* **2016**, *15*, 48–53. doi:10.1038/nmat4465
38. Li, F.; Guo, S.; Shen, J.; Shen, L.; Sun, D.; Wang, B.; Chen, Y.; Ruan, S. *Sens. Actuators, B* **2017**, *238*, 364–373. doi:10.1016/j.snb.2016.07.021
39. Choi, Y.; Stenger, H. *Fuel Chemistry Division Preprints*; Boston, 2002; pp 723–724.
40. Andersson, R.; Boutonnet, M.; Järås, S. *J. Chromatogr. A* **2012**, *1247*, 134–145. doi:10.1016/j.chroma.2012.05.060
41. dos Santos, S. G.; Varesche, M. B. A.; Zaiat, M.; Foresti, E. *Environ. Eng. Sci.* **2004**, *21*, 313–320. doi:10.1089/109287504323066950
42. Ramadan, A. A.; Gould, R. D.; Ashour, A. *Thin Solid Films* **1994**, *239*, 272–275. doi:10.1016/0040-6090(94)90863-X
43. Lin, H.; Yang, L.; Jiang, X.; Li, G.; Zhang, T.; Yao, Q.; Zheng, G. W.; Lee, J. Y. *Energy Environ. Sci.* **2017**, *10*, 1476–1486. doi:10.1039/C7EE01047H
44. Fabbri, F.; Rotunno, E.; Cinquanta, E.; Campi, D.; Bonnini, E.; Kaplan, D.; Lazzarini, L.; Bernasconi, M.; Ferrari, C.; Longo, M.; Nicotra, G.; Molle, A.; Swaminathan, V.; Salviati, G. *Nat. Commun.* **2016**, *7*, 13044. doi:10.1038/ncomms13044

## License and Terms

This is an Open Access article under the terms of the Creative Commons Attribution License (<http://creativecommons.org/licenses/by/4.0>), which permits unrestricted use, distribution, and reproduction in any medium, provided the original work is properly cited.

The license is subject to the *Beilstein Journal of Nanotechnology* terms and conditions: (<https://www.beilstein-journals.org/bjnano>)

The definitive version of this article is the electronic one which can be found at: doi:10.3762/bjnano.9.57